INORGANIC CHEMISTRY
FRONTIERS

RESEARCH ARTICLE

View Article Online
View Journal

Cite this: DOI: 10.1039/d5qi00611b

Doubly crossed supercoils built by cooperative anion and metal coordination†

Wei Zhao, *‡[a] Hongfei Li,‡[b] Xinyu Lian,‡[a] Cheng Jin,[a] Di Meng,[b] Boyang Li,[c] Xiaoyan Zheng, *[a] Xiao-Juan Yang [a] and Biao Wu*[a]

Received 1st March 2025,
Accepted 8th April 2025

DOI: 10.1039/d5qi00611b

rsc.li/frontiers-inorganic

Supercoiled structures with multiple, continuous "figure-eight" conformations, such as complex DNA plectonemes, are ubiquitous and play vital roles in biological systems. In comparison, synthetic small-molecule supercoils with two or more crossings are scarce. Herein, we report a supercoiled plectoneme structure with two crossings assembled by synergistic cation and anion coordination to a heterotopic ligand, which contains an oligourea backbone for sulfate anion coordination and two pyridyl ends for platinum(II) ion coordination. The supercoiled structure is confirmed by single-crystal diffraction to be a racemic mixture with positive and negative crossings. Enantiopure supercoils can be induced by adenosine monophosphate or inosine monophosphate binding inside the apical loops, resembling the polymerase encapsulation in bacterial plectonemes that guides DNA and RNA synthesis.

Introduction

A supercoil refers to a higher-order structure resulting from the twisting of a cyclic strand through Reidemeister moves,[1,2] which leads to uniform or opposite crossings through type I or type II moves, respectively (Fig. 1a).[3] Such conformations are frequently seen in various systems, ranging from macro- and supra-molecules to individual small molecules.[4,5] In nature, DNA supercoils (including toroidal and plectonemic structures),[6–9] formed by DNA loops, are mostly uniformly and negatively crossed (counterclockwise twist from the top view, Fig. 1a). These tertiary structures, with a condensed space, are critical for packaging, transcription and recombination of DNAs.[10,11] Within supercoil topologies, figure-eight is the simplest shape. Over the past decade, many abiotic structures with figure-eight conformations (>100 examples) have been made by inducing crossing *via* covalent bonds,[12–16] structural preorganization,[17–21] or noncovalent interactions.[22–29] As more crossings are introduced, the complexity and strain of the supercoil would increase significantly, potentially leading to new properties, such as enhanced mechanical strength or chirality.[30–33] However, creating supercoils with two or more crossings presents significant challenges, and reported examples are very limited.[34–39]

Among the known synthetic supercoils, two plectonemes resulting from type I Reidemeister move have been reported. One is a molecular-motor-derived macrocycle, which can form up to three crossings at the out-of-equilibrium state (under light irradiation).[34] The other is a thermodynamically stable, racemic plectoneme with three crossings, obtained by post-cyclization of a Cu^{+}-coordinated duplex (Fig. 1b).[36] On the other hand, through type II Reidemeister move, large macrocycles can fold into a pseudo-plectoneme structure with opposite coiling directions (positive and negative). Three such examples have been documented, involving expanded porphyrins,[37] aromatic oligoamide macrocycles,[38] and bispyrrolidinoindoline-based macrocycles.[39]

Our previous studies have indicated that *ortho*-phenylene-spaced oligourea ligands tend to form single helices (foldamers) upon coordination to anions,[41–43] which resembles the terminal loop of DNA supercoils. This led us to propose that by modifying the ends of the oligourea backbone, it would be possible to create supercoiled structures through secondary interactions, such as metal coordination. Cooperative anion and metal coordination has proven to be a promising strategy for accessing hierarchical assemblies.[44–49] Inspired by these findings, a family of oligourea ligands with varying chain lengths (hexakisurea **L**[1], pentakisurea **L**[2] and tetrakisurea **L**[3]) were designed by incorporating pyridyl groups at both ends

[a]*Key Laboratory of Medicinal Molecule Science and Pharmaceutics Engineering, Ministry of Industry and Information Technology, School of Chemistry and Chemical Engineering, Beijing Institute of Technology, Beijing 102488, China. E-mail: zhaochem@bit.edu.cn, xiaoyanzheng@bit.edu.cn, wubiao@bit.edu.cn*
[b]*Key Laboratory of Synthetic and Natural Functional Molecule Chemistry of the Ministry of Education, College of Chemistry and Materials Science, Northwest University, Xi'an 710069, China*
[c]*College of Chemistry & Pharmacy, Northwest A&F University, Yangling 712100, China*

†Electronic supplementary information (ESI) available. CCDC 2394489, 2394496, 2394994, 2394995, 2395072 and 2395079. For ESI and crystallographic data in CIF or other electronic format see DOI: https://doi.org/10.1039/d5qi00611b

‡These authors contributed equally to this work.

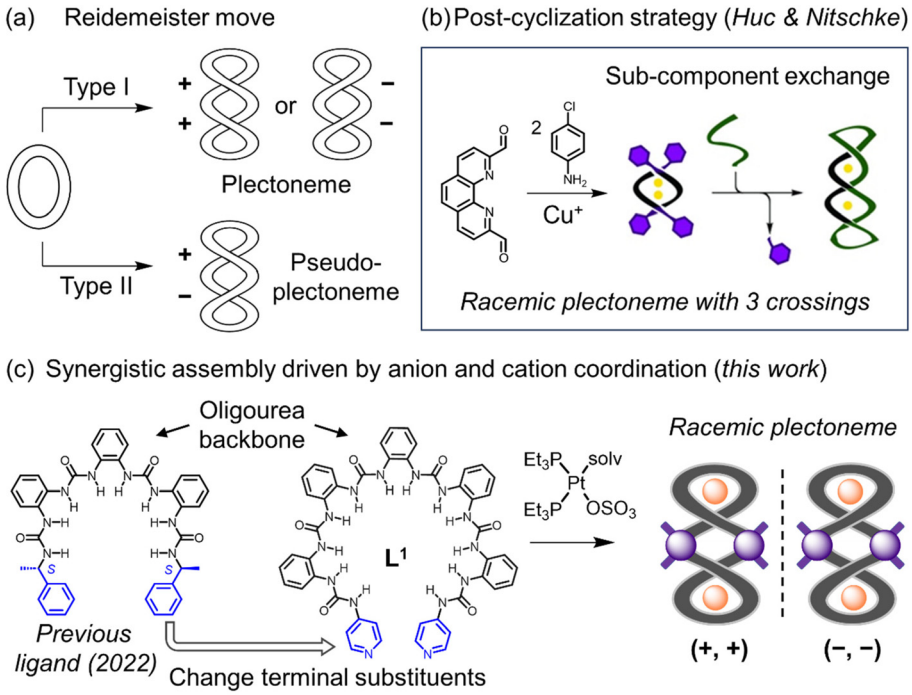

Fig. 1 (a) Schematic illustration of type I and type II Reidemeister moves of macrocyclic molecules to yield supercoiled plectonemes and pseudo-plectonemes. (b) Racemic plectoneme with three crossings made by the post-cyclization strategy. Reproduced from ref. 36 with permission from John Wiley and Sons, copyright 2009. (c) *This work*: a one-pot strategy for making plectonemes driven by SO_4^{2-} and Pt^{2+} coordination with heterotopic pyridyl-oligourea ligands. The chirality of supercoiling is indicated as (+) for positive crossing and (−) for negative crossing.[40]

(Fig. 1c). As anticipated, upon further coordination with Pt^{2+} cations, two sulfate-coordination single helices are linked to form racemic supercoils (Fig. 1c), as confirmed by single crystal structures. Moreover, the two apical loops of the prepared supercoils can selectively bind adenosine monophosphate (AMP) and inosine monophosphate (IMP) nucleotides, thus inducing enantiopure chiral supercoils.

Results and Discussion

Molecular design and anion coordination

The ligands **L**^{1}, **L**^{2} and **L**^{3} containing different oligourea moieties (number of urea groups: 6, 5 and 4) and pyridyl terminal groups were designed to study the effect of chain length on the formation of supercoils. The oligourea backbone exhibits strong anion coordination affinity, especially for oxoanions (sulfate, phosphate; up to 10^7 M^{-1} in DMSO),[42,50] thus pre-organizing a coiled conformation for further assembly. Platinum(II) was chosen as the metal center because of its stable, square-planar coordination and predictable configuration.[51] To reduce the electrostatic interaction between anion and metal cation, the *cis*-$Pt(PEt_3)_2SO_4$ complex[52] was used because sulfate ion exhibits relatively weak affinity with the Pt^{2+} cation. All three new ligands were readily synthesized and fully characterized by NMR and MS (see ESI, section S2†). The coordination of the sulfate anion to the oligourea ligands (**L**^{1}, **L**^{2} and **L**^{3}) led to the formation of single helices as confirmed by single crystal structures (Fig. S1–S3†). The sulfate ion is fully encapsulated inside the folded cavity through multiple hydrogen bonds with oligourea groups, similar to previously reported tetrakisurea ligands with other terminal groups.[41,42] Notably, the hexakisurea **L**^{1} and pentakisurea **L**^{2} are long enough to facilitate the crossing of the two terminal pyridyl groups (d_{N-N} is 11.78 Å and 11.42 Å, respectively). In contrast, the tetrakisurea backbone is too short for the pyridyls to cross.

Construction of supercoils from hexakisurea (L^1) and pentakisurea (L^2) ligands

The co-assembly by anion coordination and metal coordination was next investigated. Addition of *cis*-$Pt(PEt_3)_2SO_4$ into the solution of ligand **L**^{1}, **L**^{2} or **L**^{3} in *N*,*N*-dimethylformamide (DMF) caused precipitation, indicating the formation of supramolecular complexes. Fortunately, single crystals of these products were obtained by slow vapor diffusion of acetone to dilute DMF solutions, and the structures unambiguously confirm the formation of supercoiled plectonemes.

For the assembly of hexakisurea **L**^{1} and *cis*-$Pt(PEt_3)_2SO_4$, a supercoiled structure with two crossings is successfully obtained with an overall 2 : 2 : 2 stoichiometry of ligand, sulfate and Pt^{2+} (Fig. 2a). Each sulfate anion is encapsulated inside one terminal loop *via* eight hydrogen bonds with the oligourea backbone and two water molecules. A square-planar Pt^{2+} coordination geometry is illustrated with two triethylphosphine ligands and two pyridyl units from two distinct $[SO_4\mathbf{L}^1]^{2-}$ helices, where the *cis*-configuration is retained. The

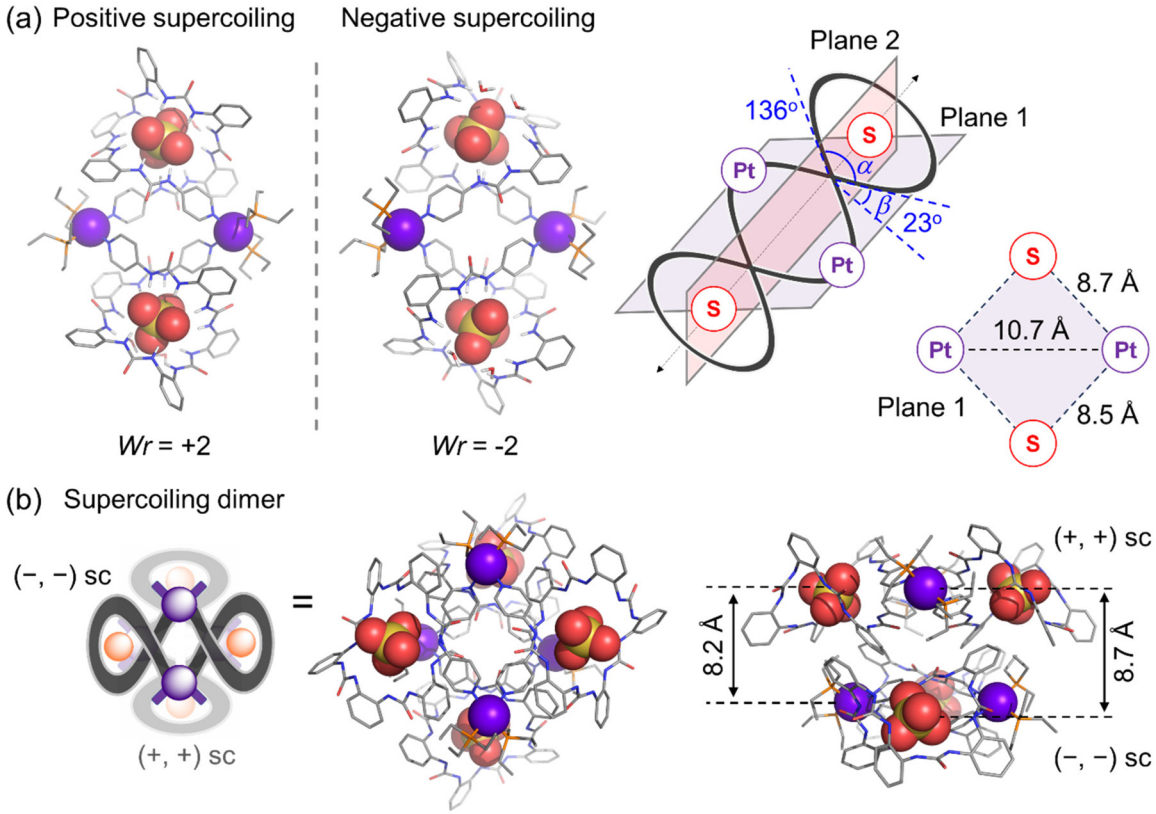

Fig. 2 Single crystal structure of supercoiled plectoneme $Pt_2\mathbf{L}^1_2(SO_4)_2$. (a) Racemic mixture of positively (+2) and negatively (−2) supercoiled plectonemes. Writhe (Wr) represents the chirality and the number of crossings, α and β indicate the crossing angle and pitch angle, respectively, and $\alpha + 2\beta \approx 180°$.[53] (b) Packing of two plectonemes with opposite crossings. Linear packing of racemic plectonemes was observed with alternating sequences along the *b* axis in solid state. Solvent molecules and nonpolar hydrogen atoms are omitted for clarity.

Pt–N bond lengths are 2.078(4) Å and 2.111(4) Å, the angle of N–Pt–N is 82.4(2)°, and the distance between two Pt atoms is 10.703(1) Å. The overall size of the $\mathbf{L}^1$-based supercoil is about 26 Å × 16 Å × 5 Å.

In the supercoiled structure, two crossings and three cavities are clearly observed. Unlike the two sulfate-encapsulated terminal cavities, the volume of the central cavity (~110 Å^3) is too small to accommodate any guest. Notably, the two ligands within one supercoil exhibit the same helical handedness, either positive (+) or negative (−), and the writhe (Wr) value (denotes the chirality and number of crossings, Fig. 2a) is determined to be +2 or −2. Therefore, a racemic mixture of (+, +) and (−, −) supercoils is produced. Presumably, this originates from the racemic structure of the $[SO_4\mathbf{L}^1]^{2-}$ helix, as seen in the crystal structure, which subsequently undergoes a narcissistic self-sorting assembly upon Pt^{2+} coordination. Such racemic supercoils have been observed in Cu^+-coordinated duplexes with three crossings, in which only two cavities can be identified with negligible volumes (no guest binding).

To further understand the supercoiled structure, the crossing is analyzed in detail. The crossing angle (α, defined as the crossover angle of the oligourea backbone, Fig. 2a) of the $\mathbf{L}^1$-based supercoil is 136°, which is larger than those of most B-DNA duplex-based supercoils (typically <90°).[53,54] This is likely attributed to the relatively high flexibility and short chain length of the oligourea backbone compared to B-DNA duplex loops. Thus, a small pitch angle (β = 23°, $\alpha + 2\beta \approx 180°$) is seen. In the structure, sulfate coordination is the main driving force for the crossover of the oligourea backbone, which is further stabilized by Pt^{2+} coordination. The two N atoms (of urea, N–Ha) next to the terminal pyridine motif exhibit the shortest distance for the crossing (~3.56 Å).

Moreover, the $\mathbf{L}^1$-based individual supercoils are linearly stacked along the *c* axis with an alternating sequence of (+, +) and (−, −) in the solid state (Fig. 2b and Fig. S5†). The distances between the metal and the anion, $d_{S\cdots Pt}$, are determined to be 8.2 Å and 8.7 Å. Two adjacent supercoils are linked through multiple C–H···π interactions (between C–H of the phenyl ring and the pyridine unit) and hydrogen bonds (sulfate–water cluster and triethylphosphine).

The structure of the $\mathbf{L}^1$-based supercoil was carefully characterized in solution based on NMR and MS techniques. First, compared to the ^{1}H NMR spectrum of free ligand $\mathbf{L}^1$ (Fig. 3a), the signals of H^1 and H^2 on the terminal pyridyl group are downfield shifted ($\Delta\delta$ (H^1) = +0.06 ppm; $\Delta\delta$ (H^2) = +0.10 ppm). This corresponds to the Pt^{2+} coordination and is consistent with typical chemical shift changes seen in other Pt^{2+}–pyridyl complexes.[52,55] In contrast, these signals do not change for the

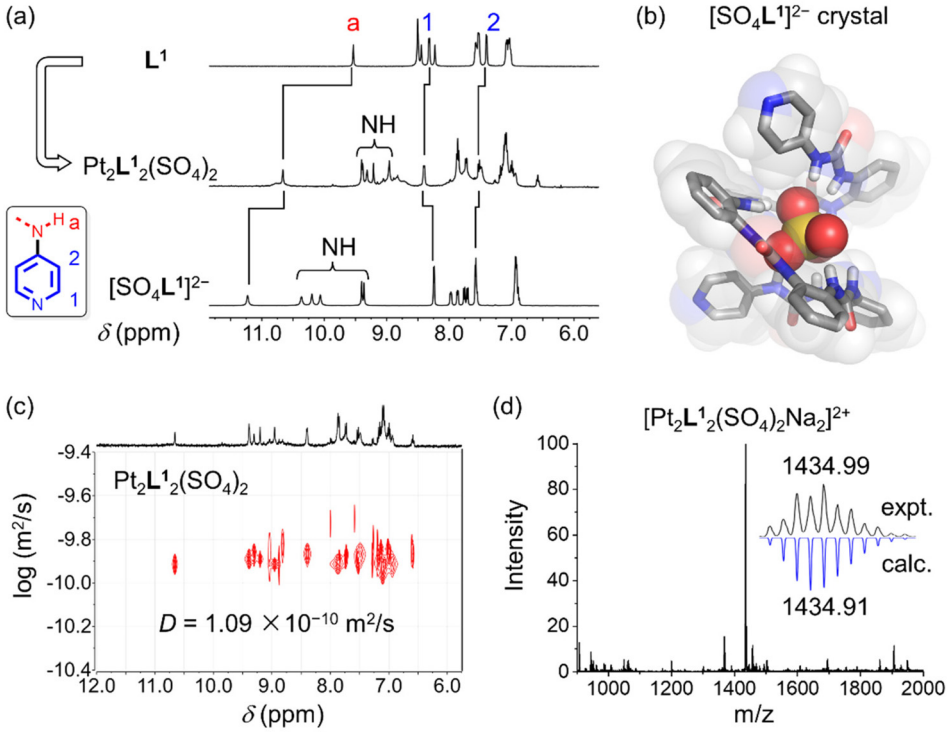

Fig. 3 (a) Stacked ^{1}H NMR spectra (1 mM, 400 MHz, DMSO-d_6, 298 K) of $\mathbf{L^1}$, $Pt_2\mathbf{L^1}_2(SO_4)_2$, and $[SO_4\mathbf{L^1}]^{2-}$ complexes. (b) Single crystal structure of the single helix $[SO_4\mathbf{L^1}]^{2-}$, tetrabutylammonium countercation and solvent molecules are omitted for clarity. (c) 2D DOSY NMR (1 mM, 400 MHz, DMSO-d_6, 298 K) and (d) ESI-MS spectra for the complex $Pt_2\mathbf{L^1}_2(SO_4)_2$.

single helix of $[SO_4\mathbf{L^1}]^{2-}$. The signals of urea N–H groups are all downfield shifted, indicating hydrogen bonding with the sulfate anion. The NH proton Ha adjacent to the pyridyl group is changed by *ca.* +1.13 ppm, which is smaller than that in the sulfate-coordinated single helix $[SO_4\mathbf{L^1}]^{2-}$ ($\Delta\delta$ = 1.70 ppm). This is because the acidity of Ha becomes weaker after Pt^{2+} coordination. Additionally, the sulfate anion is well-wrapped inside the cavity of a single helix *via* twelve hydrogen bonds with all six urea moieties, as seen in the single crystal structure (Fig. 3b). In contrast, water molecules also participate in hydrogen bonding with sulfate in the crystal structure of $\mathbf{L^1}$-based supercoils, which is consistent with the less downfield chemical shift of Ha.

2D diffusion-ordered spectroscopy (DOSY) and ESI-MS spectrometry provided further evidence for the formation of a 2 : 2 : 2 structure comprising two ligands, two sulfates and two Pt^{2+} ions. Only one species was seen in the DOSY spectrum (Fig. 3c) with a diffusion coefficient (D) of 1.09×10^{-10} m^2 s^{-1}. The calculated hydrodynamic diameter (d = 18.4 Å) is comparable with the size of the obtained supercoil in the single crystal structure (Fig. 2b). As observed from ESI-MS results, the major peak at 1434.99 is assigned to the complex $[Pt_2\mathbf{L^1}_2(SO_4)_2Na_2]^{2+}$ (Fig. 3d).

In the case of pentakisurea ligand $\mathbf{L^2}$, similar to $\mathbf{L^1}$, racemic supercoils were also obtained as suggested by the single crystal structure (Fig. 4). Specifically, the pentakisurea chain is uplifted with a relatively large helical pitch and longer Pt–Pt separation (14.5 Å *versus* 10.7 Å for $\mathbf{L^1}$-based supercoils). The shortest distance of the crossover is observed to be 5.0 Å, producing a larger central cavity for $\mathbf{L^2}$-based supercoils (volume ~250 Å^3) capable of encapsulating one acetone molecule (circled in Fig. 4). Such guest binding in all three cavities has never been observed in other supercoils before. In addition, alternating packing of positively and negatively crossed supercoils is also exhibited along the *b* axis in the solid state (Fig. 4). Yet, the packing of $\mathbf{L^2}$-based supercoils is found to be offset, with two adjacent supercoils interacting through multiple hydrogen bonds among sulfate–water clusters, triethylphosphine, and oligourea units. The co-assembly driven by anion coordination and metal coordination was also verified by ^{1}H, 2D NMR and mass spectrometry (section S6†).

Upon further reducing the chain length of the oligourea backbone to the tetrakisurea ligand $\mathbf{L^3}$, the supercoiled structure is not obtained. Instead, a macrocycle is formed with an uncoiled conformation (Fig. S8†). This is consistent with the incomplete helical turn seen in the crystal structure of the sulfate complex of $\mathbf{L^3}$ (Fig. S3†).

Compared to previously reported "figure-eight" strips, the supercoils synthesized in this study exhibit a unique structure with three consecutive circles. This configuration, featuring two crossings, is rare and closely resembles the plectonemic DNA loops induced by gyrase, which are typically found in eukaryotes and bacteria.[8,56] The obtained supercoils are driven by a combination of anion (sulfate) coordination and metal

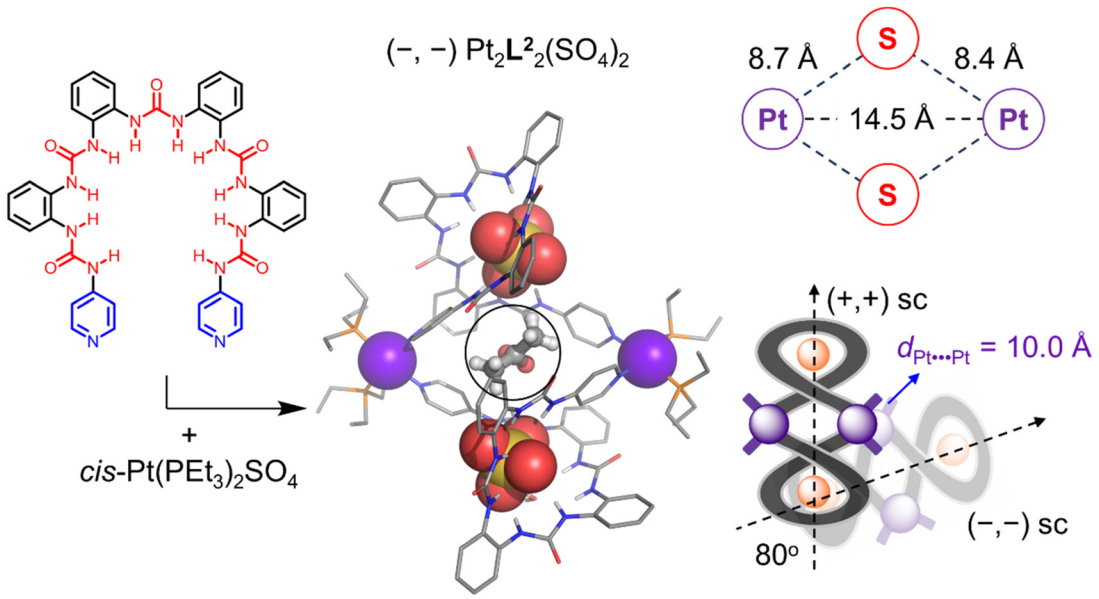

Fig. 4 Supercoiled plectoneme based on ligand L^2. Single crystal structures of (–, –) $Pt_2L^2_2(SO_4)_2$ and its dimeric packing are shown. Only negative supercoiling is shown, and one acetone molecule (circled) is encapsulated inside the central cavity. Solvent molecules and nonpolar hydrogen atoms are omitted for clarity.

(Pt^{2+}) coordination, with the former ensuring the supercoiling (*i.e.*, writhe = ±2) and the latter accomplishing the linking. In biology, one crucial function of plectonemic DNA loops is associated with the initiation of transcription activated by polymerase, which is normally encapsulated (inside the apical loops), transported, and subsequently released.[56] Inspired by this function, we examined the synthesized abiotic supercoils for potential guest binding inside the end loops. Nucleotides were targeted considering their phosphate head that bears negative charges similar to sulfate for binding with the oligourea unit, as well as their critical roles in DNA replication and RNA transcription.[57,58] Nevertheless, for potential nucleotide binding, the apical loops need to be activated by removing the pre-bound sulfate anion beforehand.

To evacuate the apical loops of plectoneme, the triflate anion (OTf^-) was used to replace sulfate because of its relatively low hydration enthalpy (−280 kJ mol^{-1}, weak binding affinity with oligourea). The plectonemes with triflate counteranions were successfully prepared either by adding $Ba(OTf)_2$ into the solution of the $Pt_2L^1_2(SO_4)_2$ complex or by mixing the pyridyl–oligourea ligand with *cis*-$Pt(PEt_3)_2(OTf)_2$ (Fig. 5a). Although single crystals were not obtained, the structure of the $[Pt_2L^1_2(OTf)_2]^{2+}$ complex was optimized by DFT calculations at the theory level of M06-2X/6-31G* (Fig. 5b), which illustrates a supercoiled conformation as a racemic mixture similar to that of the sulfate analogue.

The $[Pt_2L^1_2(OTf)_2]^{2+}$ complex was carefully characterized by NMR spectroscopy and MS spectrometry. Importantly, according to the ^1H NMR spectra (Fig. 5c), the N–H protons of oligourea are obviously upfield shifted upon triflate coordination compared to those of the sulfate-based supercoils. For example, the proton Ha is upfield shifted by about 0.5 ppm

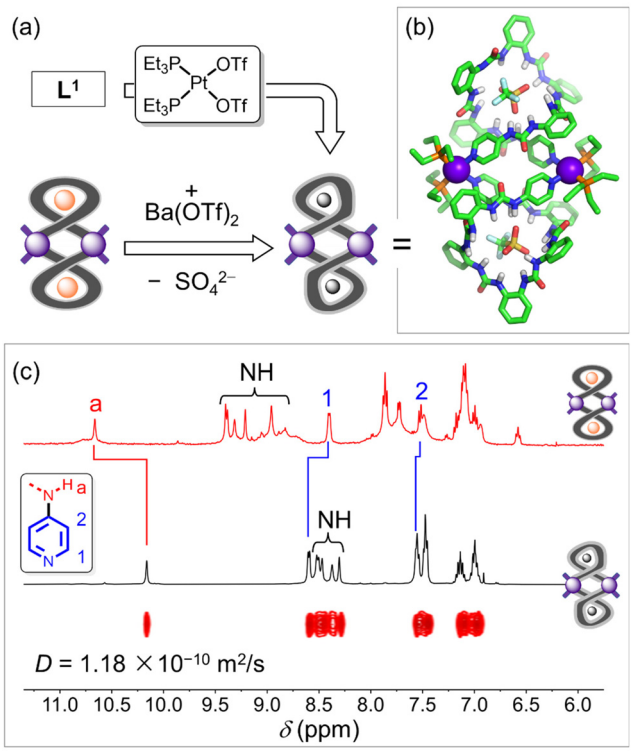

Fig. 5 (a) Schematic illustration for the preparation of a loosely supercoiled structure with the OTf^- anion. (b) DFT-optimized structure for the $[Pt_2L^1_2(OTf)_2]^{2+}$ complex with a negatively supercoiled conformation (M06-2X/6-31G*, implicit solvation: DMSO). (c) Stacked ^1H NMR spectra (1 mM, 400 MHz, DMSO-d_6, 298 K) of $[Pt_2L^1_2(OTf)_2]^{2+}$ and $Pt_2L^1_2(SO_4)_2$, and 2D DOSY NMR signals of $[Pt_2L^1_2(OTf)_2]^{2+}$ (2 mM) are shown at the bottom.

(Fig. 5c), consistent with the weaker triflate coordination. Notably, correlation signals between H^2 and N–H groups from the oligourea backbone were seen in the 2D ^1H–^1H NOESY spectrum (Fig. S25†), indicating the coiled conformation of the ligand. Similar NOE correlation signals (H^2–Hc) were also seen in sulfate-based supercoils (Fig. S23†). All these results consistently support a coiled conformation with end loops, which are available for potential guest binding.

Subsequently, guest binding properties were investigated by using phosphate-containing nucleotides. It is expected that, as the chiral nucleotide was added to the racemic supercoils, its phosphate head would bind to the oligourea loop, thus inducing supramolecular chirality with a turned-on CD response (Fig. 6a and S38†). This anion substitution occurs because the phosphate head with two negative charges has stronger binding affinity (similar to the sulfate anion binding constant, up to 10^7 M^{-1} in DMSO) for oligourea than the monoanionic triflate anion. According to the ^1H NMR spectra, the aromatic peaks reside in a region similar to those of free plectonemes (Fig. S33 and S34†), suggesting the retention of the supercoiled structure.

As desired, by adding AMP to the $[Pt_2\mathbf{L^1}_2(OTf)_2]^{2+}$ complex (Fig. 6b), a distinct CD signal in the region of 240–300 nm is identified, indicating the generation of supramolecular chirality. The CD intensity reaches a plateau by adding two equivalents of AMP, suggesting a 1 : 2 binding ratio of the supercoil with AMP guests (Fig. S43 and S44†). The Cotton effect corresponds to the absorption band at 272 nm for the oligourea backbone, which is hypochromatically shifted to 256 nm in the $[Pt_2\mathbf{L^1}_2(OTf)_2]^{2+}$ complex. This suggests the interaction between the monophosphate head group and the oligourea loop, consistent with the induction of chiral crossings. The encapsulation of AMP is also supported by ESI-MS, where a major peak at *m*/*z* 1684.44 is assigned to the $[Pt_2\mathbf{L^1}_2(AMP)_2Na_2]^{2+}$ complex (Fig. S46†). In contrast, the addition of adenosine triphosphate (ATP) and adenosine diphosphate (ADP) into the solution of $[Pt_2\mathbf{L^1}_2(OTf)_2]^{2+}$ resulted in a negligible CD response (Fig. 6b). This suggests

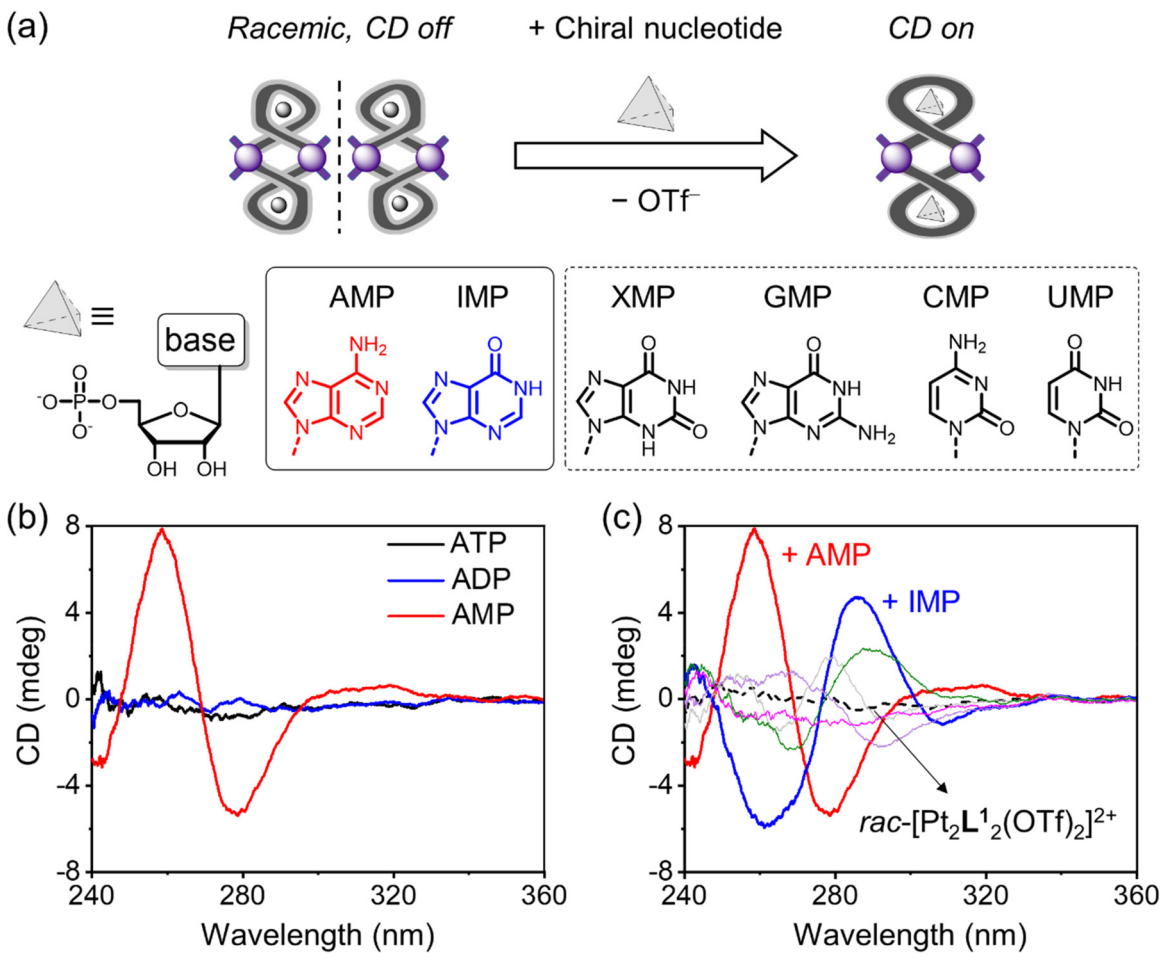

Fig. 6 (a) Schematic illustration for the chiral induction of a supercoiled plectoneme by guest nucleotide binding. Chemical structures for monophosphate nucleotides are shown below. CD responses of the *rac*-$[Pt_2\mathbf{L^1}_2(OTf)_2]^{2+}$ complex (5 μM) in the presence of (b) AMP, ADP, and ATP, and (c) AMP, IMP, and other monophosphate nucleotides. Two equivalents of nucleotides were added, and tetrabutylammonium (TBA) was used as the counter-cation for nucleotide salts (1% v/v DMSO/CH_3CN).

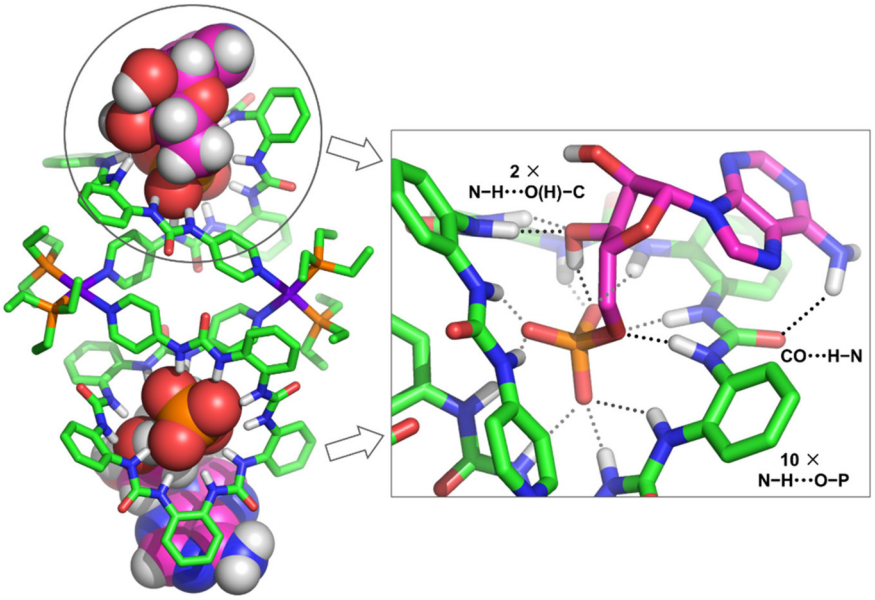

Fig. 7 DFT-optimized structure of AMP ⊂ (+, +) $\mathbf{L^1}$-based supercoils showing positively crossed conformation (M06-2X/6-31G*, implicit solvation: CH_3CN) and the multiple hydrogen bonding network of the phosphate head group and the oligourea backbone.

that the supercoils may be employed to selectively recognize AMP over ATP and ADP by CD spectroscopy.

To gain more structural information on AMP binding with the supercoils, quantum calculations were performed at the M06-2X/6-31G* level (implicit solvation, CH_3CN). Both positively and negatively supercoiled conformations in the presence of AMP were optimized, and their CD spectra were then obtained by TD-DFT calculations. Specifically, the positively supercoiled AMP ⊂ (+, +) $Pt_2\mathbf{L^1}_2$ complex is more energy favored by 126 kJ mol^{-1} than that of the negatively supercoiled AMP ⊂ (−, −) $Pt_2\mathbf{L^1}_2$ complex (M06-2X/6-31G*). In addition, the calculated CD spectrum of $(AMP)_2$ ⊂ (+, +) $\mathbf{L^1}$-based supercoils clearly matches the experimental spectrum (Fig. S50–S52† and Fig. 6b), indicating that the positively supercoiled plectoneme is favored upon AMP binding. As illustrated in Fig. 7, AMP is bound by a hydrogen bond network (13 × H-bonds) with the oligourea backbone. These include ten hydrogen bonds between the phosphate head group and urea units (N–H···O–P), two hydrogen bonds between the hydroxyl group from the sugar unit and urea (N–H···O–C), and one hydrogen bond between the amino group of the base and the urea carbonyl (N–H···O═C).

The recognition properties of the supercoils with nucleotides were also studied for five other monophosphate nucleotides with various base moieties, *i.e.*, IMP, xanthosine monophosphate (XMP), guanosine monophosphate (GMP), cytidine monophosphate (CMP), and uridine monophosphate (UMP). Only the addition of the IMP nucleotide could induce a distinct Cotton effect in the region of 240–300 nm, while adding all four of the other nucleotides results in a negligible CD response (Fig. 6c). Nearly opposite Cotton effects are recorded by adding AMP and IMP into the *rac*-supercoils. AMP binding induces the maximum positive Cotton effect (+7.9 mdeg) at 259 nm and the minimum negative Cotton effect (−5.3 mdeg) at 279 nm. IMP binding induces the maximum positive Cotton effect (+4.7 mdeg) at 286 nm and the minimum negative Cotton effect (−5.8 mdeg) at 261 nm. Although AMP and IMP contain the same stereocenter of the sugar moiety, the base unit likely guides the ultimate chirality of supercoils. Overall, the loop-activated supercoils could be utilized to differentiate monophosphate nucleotides from the di- and tri-phosphate analogues. Such selective nucleotide binding clearly resembles the polymerase binding by plectonemic DNA loops as demonstrated in bacteria.[56]

Conclusions

In summary, we have developed a novel approach for synthesizing supercoils with two crossings by cooperative coordination of anions (sulfate) and metals (Pt^{2+}) using oligourea–pyridyl ligands. Moreover, enantiopure supercoils were induced upon binding of adenosine monophosphate or inosine monophosphate to the terminal loops, which closely mimics the polymerase encapsulation in DNA supercoils found in bacteria. Given the structural complexity and adaptability of these supercoils, this work paves the way for the molecular design of high-level topologies, advanced materials, and the development of synthetic systems that replicate biological processes.

Author contributions

B. W., W. Z. and H. L. designed and supervised the research. H. L., C. J., D. M., and B. L. carried out all the experimental work, including synthesis, preparation of supercoiling

assemblies, characterization, and other data collections. X. L. performed the DFT calculations under the supervision of X. Z. W. Z., X.-J. Y. and B. W. prepared the manuscript with input from all the authors.

Data availability

Synthetic details, characterization studies of all compounds, NMR, mass spectrometry, and X-ray diffraction data are included in the ESI.† Deposition numbers 2394489 (for $\mathbf{L}^1$-based supercoils), 2394496 (for $\mathbf{L}^2$-based supercoils), 2394994 (for $\mathbf{L}^3$-based supramolecular macrocycles), 2394995 (for $\mathbf{L}^2$-based foldamers), 2395072 (for $\mathbf{L}^3$-based foldamers), and 2395079 (for $\mathbf{L}^1$-based foldamers) contain the supplementary crystallographic data for this paper.

Conflicts of interest

The authors declare no competing interests.

Acknowledgements

This work was supported by the National Natural Science Foundation of China (22101024 and 22171023) and the Beijing Municipal Natural Science Foundation (2222025). We also acknowledge the support from the Analysis & Testing Center of the Beijing Institute of Technology for data collection.

References

1 J. W. Alexander and G. B. Briggs, On Types of Knotted Curves, *Ann. Math.*, 1926, **28**, 562.
2 K. Reidemeister, Elementare Begründung der Knotentheorie, *Abh. Math. Semin. Univ. Hamburg*, 1927, **5**, 24.
3 S. D. P. Fielden, D. A. Leigh and S. L. Woltering, Molecular Knots, *Angew. Chem., Int. Ed.*, 2017, **56**, 11166.
4 V. Haridas, H. Singh, Y. K. Sharma and K. Lal, Engineering macrocyclic figure-eight motif, *J. Chem. Sci.*, 2007, **119**, 219.
5 M. Diener, J. Adamcik, A. Sánchez-Ferrer, F. Jaedig, L. Schefer and R. Mezzenga, Primary, Secondary, Tertiary and Quaternary Structure Levels in Linear Polysaccharides: From Random Coil, to Single Helix to Supramolecular Assembly, *Biomacromolecules*, 2019, **20**, 1731.
6 S. M. Mirkin, in *eLS*, 2001, DOI: 10.1038/npg.els.0001038.
7 J. R. Stagno, B. Ma, J. Li, A. S. Altieri, R. A. Byrd and X. Ji, Crystal structure of a plectonemic RNA supercoil, *Nat. Commun.*, 2012, **3**, 901.
8 A. Noy, T. Sutthibutpong and S. A. Harris, Protein/DNA interactions in complex DNA topologies: expect the unexpected, *Biophys. Rev.*, 2016, **8**, 233.
9 C. Dekker, C. H. Haering, J.-M. Peters and B. D. Rowland, How do molecular motors fold the genome?, *Science*, 2023, **382**, 646.
10 M. Nöllmann, M. D. Stone, Z. Bryant, J. Gore, N. J. Crisona, S.-C. Hong, S. Mitelheiser, A. Maxwell, C. Bustamante and N. R. Cozzarelli, Multiple modes of Escherichia coli DNA gyrase activity revealed by force and torque, *Nat. Struct. Biol.*, 2007, **14**, 264.
11 I. D'Annessa, A. Coletta, T. Sutthibutpong, J. Mitchell, G. Chillemi, S. Harris and A. Desideri, Simulations of DNA topoisomerase 1B bound to supercoiled DNA reveal changes in the flexibility pattern of the enzyme and a secondary protein–DNA binding site, *Nucleic Acids Res.*, 2014, **42**, 9304.
12 F. Lin, H.-Y. Peng, J.-X. Chen, D. T. W. Chik, Z. Cai, K. M. C. Wong, V. W. W. Yam and H. N. C. Wong, Synthesis and Photophysical Studies of Chiral Helical Macrocyclic Scaffolds via Coordination-Driven Self-Assembly of 1,8,9,16-Tetraethynyltetraphenylene. Formation of Monometallic Platinum(II) and Dimetallic Platinum(II)–Ruthenium(II) Complexes, *J. Am. Chem. Soc.*, 2010, **132**, 16383.
13 W. Xu, X.-D. Yang, X.-B. Fan, X. Wang, C.-H. Tung, L.-Z. Wu and H. Cong, Synthesis and Characterization of a Pentiptycene-Derived Dual Oligoparaphenylene Nanohoop, *Angew. Chem., Int. Ed.*, 2019, **58**, 3943.
14 S.-N. Lei, H. Xiao, Y. Zeng, C.-H. Tung, L.-Z. Wu and H. Cong, BowtieArene: A Dual Macrocycle Exhibiting Stimuli-Responsive Fluorescence, *Angew. Chem., Int. Ed.*, 2020, **59**, 10059.
15 L. Zhan, C. Dai, G. Zhang, J. Zhu, S. Zhang, H. Wang, Y. Zeng, C.-H. Tung, L.-Z. Wu and H. Cong, A Conjugated Figure-of-Eight Oligoparaphenylene Nanohoop with Adaptive Cavities Derived from Cyclooctatetrathiophene Core, *Angew. Chem., Int. Ed.*, 2022, **61**, e202113334.
16 R. Katoono, S. Kawai, K. Fujiwara and T. Suzuki, Controllability of dynamic double helices: quantitative analysis of the inversion of a screw-sense preference upon complexation, *Chem. Sci.*, 2015, **6**, 6592.
17 J.-I. Setsune, A. Tsukajima, N. Okazaki, J. M. Lintuluoto and M. Lintuluoto, Enantioselective Induction of Helical Chirality in Cyclooctapyrroles by Metal-Complex Formation, *Angew. Chem., Int. Ed.*, 2009, **48**, 771.
18 Z. Zhang, W.-Y. Cha, N. J. Williams, E. L. Rush, M. Ishida, V. M. Lynch, D. Kim and J. L. Sessler, Cyclo[6]pyridine[6]pyrrole: A Dynamic, Twisted Macrocycle with No Meso Bridges, *J. Am. Chem. Soc.*, 2014, **136**, 7591.
19 K. Liang, H. Chen, X. Wang, T. Lu, Z. Duan, J. L. Sessler and C. Lei, Di-2,7-pyrenidecaphyrin(1.1.0.0.0.1.1.0.0.0) and Its Bis-Organopalladium Complexes: Synthesis and Chiroptical Properties, *Angew. Chem., Int. Ed.*, 2023, **62**, e202212770.
20 Q. Zhou, X. Hou, J. Wang, Y. Ni, W. Fan, Z. Li, X. Wei, K. Li, W. Yuan, Z. Xu, M. Zhu, Y. Zhao, Z. Sun and J. Wu, A Fused [5]Helicene Dimer with a Figure-Eight Topology: Synthesis, Chiral Resolution, and Electronic Properties, *Angew. Chem., Int. Ed.*, 2023, **62**, e202302266.
21 Q. Zhou, W. Yuan, Y. Li, Y. Han, L. Bao, W. Fan, L. Jiao, Y. Zhao, Y. Ni, Y. Zou, H.-B. Yang and J. Wu, [5]Helicene Based π-Conjugated Macrocycles with Persistent Figure-

Eight and Möbius Shapes: Efficient Synthesis, Chiral Resolution and Bright Circularly Polarized Luminescence, *Angew. Chem., Int. Ed.*, 2024, e202417749.
22 D. Meshcheryakov, V. Böhmer, M. Bolte, V. Hubscher-Bruder, F. Arnaud-Neu, H. Herschbach, A. Van Dorsselaer, I. Thondorf and W. Mögelin, Two Chloride Ions as a Template in the Formation of a Cyclic Hexaurea, *Angew. Chem., Int. Ed.*, 2006, **45**, 1648.
23 Y. Nakatani, Y. Furusho and E. Yashima, Synthesis of helically twisted [1 + 1]macrocycles assisted by amidinium–carboxylate salt bridges and control of their chiroptical properties, *Org. Biomol. Chem.*, 2013, **11**, 1614.
24 R. Costil, S. Crespi, L. Pfeifer and B. L. Feringa, Modulation of a Supramolecular Figure-of-Eight Strip Based on a Photoswitchable Stiff-Stilbene, *Chem. – Eur. J.*, 2020, **26**, 7783.
25 G. Zhao, S.-Q. Chen, W. Zhao, B. Li, W. Zhang, B. Zheng, X.-J. Yang and B. Wu, Modular Synthesis of Tetraurea and Octaurea Macrocycles Encoded with Specific Monomer Sequences, *CCS Chem.*, 2021, 2692.
26 Z. Cui, X. Gao, Y.-J. Lin and G.-X. Jin, Stereoselective Self-Assembly of Complex Chiral Radial [5]Catenanes Using Half-Sandwich Rhodium/Iridium Building Blocks, *J. Am. Chem. Soc.*, 2022, **144**, 2379.
27 J.-F. Ayme, B. Bruchmann, L. Karmazin and N. Kyritsakas, Transient self-assembly of metal–organic complexes, *Chem. Sci.*, 2023, **14**, 1244.
28 F. Niess, V. Duplan and J.-P. Sauvage, Interconversion between a Vertically Oriented Transition Metal-Complexed Figure-of-Eight and a Horizontally Disposed One, *J. Am. Chem. Soc.*, 2014, **136**, 5876.
29 L.-L. Dang, Z.-B. Sun, W.-L. Shan, Y.-J. Lin, Z.-H. Li and G.-X. Jin, Coordination-driven self-assembly of a molecular figure-eight knot and other topologically complex architectures, *Nat. Commun.*, 2019, **10**, 2057.
30 Q. Li, G. Fuks, E. Moulin, M. Maaloum, M. Rawiso, I. Kulic, J. T. Foy and N. Giuseppone, Macroscopic contraction of a gel induced by the integrated motion of light-driven molecular motors, *Nat. Nanotechnol.*, 2015, **10**, 161.
31 C. Gao, A. Vargas Jentzsch, E. Moulin and N. Giuseppone, Light-Driven Molecular Whirligig, *J. Am. Chem. Soc.*, 2022, **144**, 9845.
32 J. M. Fogg, A. K. Judge, E. Stricker, H. L. Chan and L. Zechiedrich, Supercoiling and looping promote DNA base accessibility and coordination among distant sites, *Nat. Commun.*, 2021, **12**, 5683.
33 G. R. Kiel, K. L. Bay, A. E. Samkian, N. J. Schuster, J. B. Lin, R. C. Handford, C. Nuckolls, K. N. Houk and T. D. Tilley, Expanded Helicenes as Synthons for Chiral Macrocyclic Nanocarbons, *J. Am. Chem. Soc.*, 2020, **142**, 11084.
34 M. Kathan, S. Crespi, N. O. Thiel, D. L. Stares, D. Morsa, J. de Boer, G. Pacella, T. van den Enk, P. Kobauri, G. Portale, C. A. Schalley and B. L. Feringa, A light-fuelled nanoratchet shifts a coupled chemical equilibrium, *Nat. Nanotechnol.*, 2022, **17**, 159.
35 M. Hutin, C. A. Schalley, G. Bernardinelli and J. R. Nitschke, Helicate, Macrocycle, or Catenate: Dynamic Topological Control over Subcomponent Self-Assembly, *Chem. – Eur. J.*, 2006, **12**, 4069.
36 V. E. Campbell, X. de Hatten, N. Delsuc, B. Kauffmann, I. Huc and J. R. Nitschke, Interplay of Interactions Governing the Dynamic Conversions of Acyclic and Macrocyclic Helicates, *Chem. – Eur. J.*, 2009, **15**, 6138.
37 J.-I. Setsune, Y. Katakami and N. Iizuna, [48]Dodecaphyrin-(1.0.1.0.1.0.1.0.1.0.1.0) and [64]Hexadecaphyrin-(1.0.1.0.1.0.1.0.1.0.1.0.1.0.1.0): The Largest Cyclopolypyrroles, *J. Am. Chem. Soc.*, 1999, **121**, 8957.
38 C. Yao, B. Kauffmann, I. Huc and Y. Ferrand, Self-assembling figure-of-eight and pseudoplectoneme aromatic oligoamide ribbons, *Chem. Commun.*, 2022, **58**, 5789.
39 T. Honda, D. Ogata, M. Tsurui, S. Yoshida, S. Sato, T. Muraoka, Y. Kitagawa, Y. Hasegawa, J. Yuasa and H. Oguri, Rapid Synthesis of Chiral Figure-Eight Macrocycles Using a Preorganized Natural Product-Based Scaffold, *Angew. Chem., Int. Ed.*, 2024, **63**, e202318548.
40 J. E. Deweese, M. A. Osheroff and N. Osheroff, DNA topology and topoisomerases, *Biochem. Mol. Biol. Educ.*, 2009, **37**, 2.
41 C. Jia, B. Wu, S. Li, X. Huang and X.-J. Yang, Tetraureas versus Triureas in Sulfate Binding, *Org. Lett.*, 2010, **12**, 5612.
42 B. Wu, C. Jia, X. Wang, S. Li, X. Huang and X.-J. Yang, Chloride Coordination by Oligoureas: From Mononuclear Crescents to Dinuclear Foldamers, *Org. Lett.*, 2012, **14**, 684.
43 H. Li, L. Kou, L. Liang, B. Li, W. Zhao, X.-J. Yang and B. Wu, Anion-coordination-driven single–double helix switching and chiroptical molecular switching based on oligoureas, *Chem. Sci.*, 2022, **13**, 4915.
44 C. R. Bondy, P. A. Gale and S. J. Loeb, Metal–Organic Anion Receptors: Arranging Urea Hydrogen-Bond Donors to Encapsulate Sulfate Ions, *J. Am. Chem. Soc.*, 2004, **126**, 5030.
45 D. J. Mercer and S. J. Loeb, Metal-based anion receptors: an application of second-sphere coordination, *Chem. Soc. Rev.*, 2010, **39**, 3612.
46 F. Cui, S. Li, C. Jia, J. S. Mathieson, L. Cronin, X.-J. Yang and B. Wu, Anion-Dependent Formation of Helicates versus Mesocates of Triple-Stranded M2L3 (M = Fe2+, Cu2+) Complexes, *Inorg. Chem.*, 2012, **51**, 179.
47 A. Thevenet, R. Custelcean, B. A. Moyer and S. Jansone-Popova, Synergistic Self-Assembly of Oxoanions and d-Block Metal Ions with Heteroditopic Receptors into Triple-Stranded Helicates, *Chem. – Eur. J.*, 2020, **26**, 14290.
48 Y. Liu, Z. Jiang, Y. Guan, Q. Bai, Z. Zhang, Y. Li, H. Zhao, T.-Z. Xie, M. Wang, P. Wang and T. Wu, Halide ion directed templation effect of quadruple-stranded helicates, *Cell Rep. Phys. Sci.*, 2022, **3**, 101056.
49 L. Zhang, B. Li, R. Li, Y. Wang, S. Ye, P. Zhang and B. Wu, Spontaneous Resolution of Chiral Janus-Type Double-Layered Metallocyclic Strips Incorporating Möbius Ring and Circular Helicate, *J. Am. Chem. Soc.*, 2023, **145**, 18221.
50 L. Liang, W. Zhao, X.-J. Yang and B. Wu, Anion-Coordination-Driven Assembly, *Acc. Chem. Res.*, 2022, **55**, 3218.

51 M. A. Soto and M. J. MacLachlan, Responsive macrocyclic and supramolecular structures powered by platinum, *Chem. Sci.*, 2024, **15**, 431.
52 W. Zheng, W. Wang, S.-T. Jiang, G. Yang, Z. Li, X.-Q. Wang, G.-Q. Yin, Y. Zhang, H. Tan, X. Li, H. Ding, G. Chen and H.-B. Yang, Supramolecular Transformation of Metallacycle-linked Star Polymers Driven by Simple Phosphine Ligand-Exchange Reaction, *J. Am. Chem. Soc.*, 2019, **141**, 583.
53 S. S. Zakharova, W. Jesse, C. Backendorf, S. U. Egelhaaf, A. Lapp and J. R. C. van der Maarel, Dimensions of Plectonemically Supercoiled DNA, *Biophys. J.*, 2002, **83**, 1106.
54 Y. Timsit and P. Várnai, Helical Chirality: a Link between Local Interactions and Global Topology in DNA, *PLoS One*, 2010, **5**, e9326.
55 G. Li, Z. Zhou, C. Yuan, Z. Guo, Y. Liu, D. Zhao, K. Liu, J. Zhao, H. Tan and X. Yan, Trackable Supramolecular Fusion: Cage to Cage Transformation of Tetraphenylethylene-Based Metalloassemblies, *Angew. Chem., Int. Ed.*, 2020, **59**, 10013.
56 A. Travers and G. Muskhelishvili, A common topology for bacterial and eukaryotic transcription initiation?, *EMBO Rep.*, 2007, **8**, 147.
57 L. Zhao, L. Cheng, Y. Yang, P. Wang, P. Tian, T. Yang, H. Nian and L. Cao, Biomimetic Hydrogen-Bonded G·C·G·C Quadruplex within a Tetraphenylethene-Based Octacationic Spirobicycle in Water, *Angew. Chem., Int. Ed.*, 2024, **63**, e202405150.
58 Q. Li, C. Yan, P. Zhang, P. Wang, K. Wang, W. Yang, L. Cheng, D. Dang and L. Cao, Tetraphenylethene-Based Molecular Cage with Coenzyme FAD: Conformationally Isomeric Complexation toward Photocatalysis-Assisted Photodynamic Therapy, *J. Am. Chem. Soc.*, 2024, **146**, 30933.